University of Alberta
Autonomous Robotic Vehicle Project
RoboSub 2017 Journal Paper

Rumman Waqar - Project Lead, Randi Derbyshire - Business Team Co-Lead, Jonathon Machinski - Business Team Co-Lead, Parsa Amini - Mechanical Team Lead, Brayden DeBoon - Electrical Team Lead, Noni Hua - Software Team Lead, Sean Scheideman, Sean Haliburton, James Hryniw, Jesse Tham, Jin Jun, Jacky Chung, Brad Hesson, Andrew Schroeder, Eric Wells, Alain Letourneau, Farez Halim, Moira Blenkinsopp, Nicholas Kraemer, Curtis Stewart, Ryan van Drecht, Mike Bardwell, Brendan Calef

***Abstract*—The paper presented details the design choices and experimental trials that resulted in Auri, the new robot by the Autonomous Robotic Vehicle Project for RoboSub 2017. With a new robot and team structure, the team is more agile and financially stable than ever before. The result is a robot redesigned to far exceed the mechanical, electrical and software capabilities of its ancestors.**

I. INTRODUCTION

This year the Autonomous Robotic Vehicle Project's goal was to address the failings of the previous robot, AquaUrsa, while expanding on its strengths. The mechanical design was intended to eliminate the the robot's weight issue by narrowing the hull, while keeping the previous design's cylindrical fortitude. The design also allowed us to access our electrical components without risking damage to the systems. Electrically, the team aimed for a revamped power system that eliminated variability, and would be able to deliver power from new lower voltage batteries, while powering many new and redesigned onboard systems. Software-wise, focus was placed on algorithms for navigation, computer vision, and deep learning. Finally, a dedicated business team was created, giving ARVP a new financial foundation to succeed this year and in the future.

II. SOFTWARE

Auri's software system is composed of several distinct modules; *Sensor Drivers*, *Computer Vision*, *Mission Planning* and *Diagnostics*. All these components are connected through the Robot Operating System (ROS), an open source communications library. ROS was chosen as a software framework because it supports a highly distributed system, which lets Auri maximize the use of its two onboard computers. In addition, ROS nodes empower the software team to create modular code and consistent I/O endpoints, which have been invaluable to the development process. By leveraging each component separately, different techniques can be evaluated and iterated on quickly. For example, swapping computer vision algorithms at runtime to determine the best performing one given current conditions.

Auri's system's are distributed over two computers: the Nvidia Jetson TX2 and the Odroid C2. The two computers coordinate over the ROS communication protocol to split up the computational workload of the software tasks. Intensive computer vision computations are ran on the Jetson to take advantage of its graphics processing unit (GPU). The Odroid handles the rest of the tasks, which includes gathering sensor data, updating the PID controllers, and monitoring the mission planner.

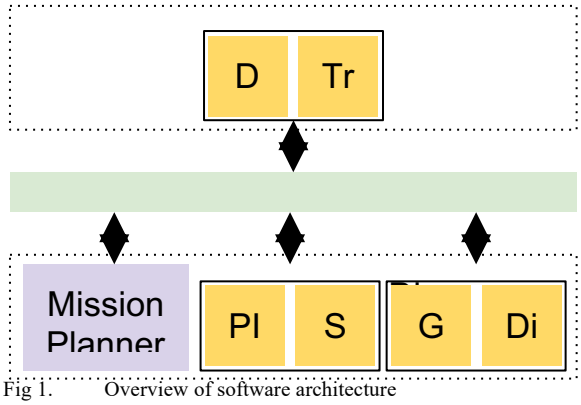

Fig 1. Overview of software architecture

A. Control System

Auri's control system is the low-level framework that handles all of its movement and data collection processes. The first part is a collection of custom-made interfaces for all Auri's sensors and motors,

allowing each device to interoperate easily with higher-level software components. Among others, the drivers are responsible for initializing a device, communicating with it via the appropriate protocol, and passing information between devices and higher-level software components using ROS messages. Currently implemented drivers include:

- A depth sensor driver that interfaces with the pressure transducer and informs other components of the measured depth.
- A heading and acceleration driver that communicates with the compass, accelerometer, and gyroscope, providing other components with tilt-compensated heading and acceleration information.
- A motor controller driver that accepts motor commands and generates the PWM and direction signals required by each of the thrusters.
- A sonar driver that receives the time-differences-of-arrival of incoming sonar signals, and provides the results to the high-level sonar localization components.
- A frame-grabbing driver that captures camera stills and provides them to the image processing components.

B. Computer Vision

This year, ARVP has made enormous strides in developing a computer vision system for Auri. Since these algorithms from previous years have never worked during the competition, it needed to be completely redeveloped keeping in mind two key principals: all new algorithms should work equally well during pool tests and on competition footage, and dependence on color should minimized or eliminated. This is because underwater image processing is affected by light attenuation and scattering, which results in poor contrast and non-uniform colors [1]. Instead, Auri's new vision algorithms use the shapes of the competition objects (eg, Buoy, path, gate), which are more reliable indicators. In light of a completely revamped architecture, this year's two main goals are to accomplish the buoy task and to follow the path. The three main vision algorithms used for target localization are:

- Contour based shape detection
- Parameterless Ellipse fitting
- Deep Learning

The vision algorithms are implemented using the OpenCV library [3] as well as LAPACK [4], a linear algebra package. To utilize the full capabilities of the Jetson TX2, the algorithms have been optimized for use on a GPU, especially when it comes to deep learning.

i. Contour based shape detection

The simplest method for identifying circular and rectangular objects without color dependance is contour detection. Using OpenCV's Canny edge detector and HoughCircles function, rectangles and circles can be extracted from high-contrast images and filtered by their basic geometric features. This is useful for a multitude of tasks, from the path and marker bins to the torpedo targets.

ii. Parameterless Ellipse fitting

Combining a shape detector and a shape filter, parameterless ellipse fitting is a robust detection system for many elementary geometric shapes. For the competition, this technique is used to find the geometric center of buoys within the field of view and provides a viable alternative to deep learning techniques for buoy detection and classification. Fig. 2 outlines the basic detection schema.

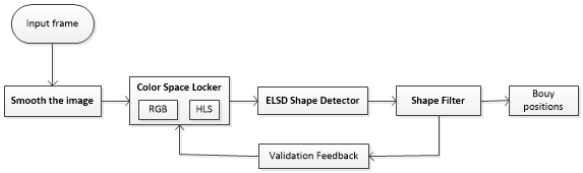

Fig 2. Parameterless Ellipse Fitting Overview

The method begins by extracting elliptical arc contours from an image using an Ellipse and Line Segment (ELSD) detector [10]. The detector obeys a 3-step scheme: candidate selection, candidate validation, and model selection. The latter two are formally sound, being grounded on statistical foundations [10]. Only the candidate selection is heuristic, for efficiency reasons.

Once a set of candidate line segments and elliptical arcs have been collected, they are filtered for positive matches. Considering the simple vision environment underwater, it's possible to design a shape filter based on some simple criteria. A buoy candidate must:

- be an elliptical arc,
- have a descriptive relationship between its start angle and end angle, and
- exceed a minimum size threshold.

While computationally expensive in conventional swimming pools, where candidates are plentiful, it proves much more accurate and efficient in the low-feature, low-contrast environment of the competition pool similar to Fig 3. To get valid detections at very long distances like those on the right of Fig 3, the detector switches from running on gray-scale imagery to using the saturation channel in HLS (or HSV) color space[1].

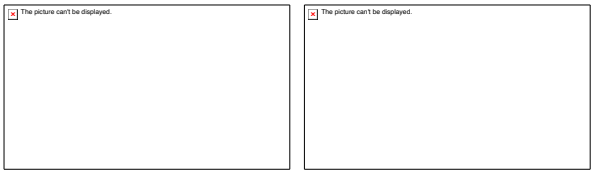

Fig 3. [Left] - Detection with caustics. [Right] - Detection from far away

iii. Deep learning

Another method used for object detection was deep learning. Deep learning refers to using artificial neural networks with more than one hidden layer to learn a function from training data. The advantage of deep learning is that it takes raw data as input and with enough training data can generalize well to a variety of scenes and conditions.

A major concern when choosing a deep learning framework and model was deploying the trained model on the Jetson TX2. As a result two frameworks that would be easy to deploy were chosen for comparison: Darknet+YOLO [11] and Digits+Caffe+DetectNet [12]. Darknet is written in C so is can be integrated into Auri's existing C++ vision code and for DetectNet, NVIDIA has a inference library called TensorRT with a C++ api for deploying trained Caffe models on the TX2. In addition, both these methods can be trained for multiple classes.

In order to compare the two frameworks, the first models were trained to detect only the red buoy. The datasets used for training and testing are a combination of all ARVP's videos from past competitions as well as from the University of Alberta pool and split into training, validation and test sets. For the red buoy, there are 4386 training images, 1096 validation images and 1326 testing images. All the training was done on a AWS instance with one NVIDIA K80 GPU. Below, Table. I shows how each model performed on the test set.

Table I

DEEP LEARNING MODEL COMPARISON FOR RED BUOY CLASS.

Model	IoU (avg)	Precision	Recall	Accuracy	Fps
DetectNet	77.79	96.38	96.26	94.49	4
Tiny YOLO	61.33	84.73	89.98	79.94	8
YOLO	77.18	90.56	99.55	99.54	3

A intersection over union (IoU) of 50% was used to determine if a detection was correct when compared with the ground truth. Overall YOLO is the most accurate but DetectNet has higher precision. Tiny YOLO performs the worst out of the three, which is not surprising given that it is a smaller network. However, it has the fastest inference speed on the TX1 at 8 frames per second (Fps). The main problem with the Tiny YOLO model is the inaccurate bounding box size it estimates. If a 0.3 IoU threshold is used instead, the accuracy increases to 90%. Fig. 3 shows some different situations where the models succeeded.

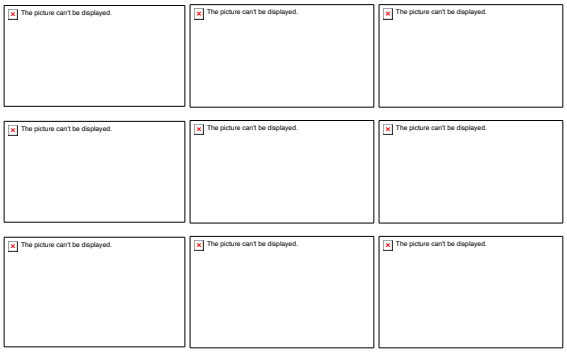

Fig. 4. [Top row] -Detection with caustics on the buoy, [Middle row] - Detection in darker condition, [Bottom row] - Detection from far away and with poor visibility

As shown the initial results of applying deep learning to this problem are positive, therefore the

[1] Full size images are provided in Appendix B.

team is moving forward with labelling the rest of the buoys and front path. In regards to improving processing speed, both YOLO models resize the image to 416X416 resolution before being processed by the network and therefore increasing the inference speed without lowering the accuracy is unlikely for Darknet as the input image resolution is already quite small. Whereas, DetectNet processes the original 1280X704 resolution image as input; therefore, decreasing the image resolution could increase the processing speed for that model and this will be experimented with in the future.

iv. Deep learning with Synthetic Images

Another test performed was using synthetic images from a simulator, to train the deep learning object detection model. This experiment was inspired by the work of Shafaei et al. who used densely labeled images generated by video games to train a image segmentation models [14]. The reason for exploring this is to generate images of objects that ARVP has very little training data for. For example ARVP's database of images has a large number of buoy images, but there are fewer with the path in them, and none with the torpedo target, or bins. In addition a simulator makes it easy to produce training data under a variety of different conditions ie. variable illumination, fog density, and caustic intensity. Ideally this will lead to a more robust detector. Finally the Unity simulator has been set up to automatically label the generated images removing the tedious task of labeling images by hand, the Unity project is discussed further in Section *D*.

For testing, two additional YOLO models were trained for red buoy detection, one with just synthetic images, and another with synthetic and real images. A comparison of these models and the initial model trained on only real images is shown in Table II.. The results show that the accuracy when training with only synthetic images is poor, suggesting that the Unity simulator is not photorealistic enough. However, when trained on both synthetic and real images the number of false positives decreases, increasing the precision by 8%, and with only a 1% drop in overall accuracy. While the results below are very encouraging, further experiments need to be performed with multiclass models.

Table II

YOLO MODEL COMPARISON WITH SYNTHETIC DATA FOR RED BUOY CLASS.

Dataset	IoU (avg)	Precision	Recall	Accuracy
Real	77.18	90.56	99.55	99.54
Synthetic	60.34	88.42	47.71	45.48
Real + Synthetic	75.28	98.57	99.16	98.49

C. Mission Planner

While attempting to outline an increasingly complex series of tasks this year, the software team quickly discovered that the old mission planning codebase was too large and error-prone. Prompted by these difficulties, the team decided that high-level control of robot operations should be handled by a single hierarchical state-machine. The software team selected SMACH[9], an open source ROS package, for this task to ensure an extensible structure and robust error handling.

A major success of this year's mission planner is its simplicity. With the bulk of the application logic modularized in ROS action and service clients, the mission planner's only concern is top-level logic, calling child nodes and piping data from one process to another. Additionally, SMACH's hierarchical structure allows each task to be a state machine which can be added to other state machines, further simplifying readability and maintainability. One nice-to-have feature of the SMACH library is the ability to visualize states and state transitions as a high-level flowchart. Not only does this mean implementing new tasks is an intuitive process, but also that coded states can easily be debugged and compared against pre-drawn plans.As such, implementing complex behavior has become feasible. For instance, when the tracker loses a buoy it makes the appropriate transition to attempt a re-detection or begin a search pattern to relocate it. Below in Fig. 5 is the state machine design used for the buoy task.

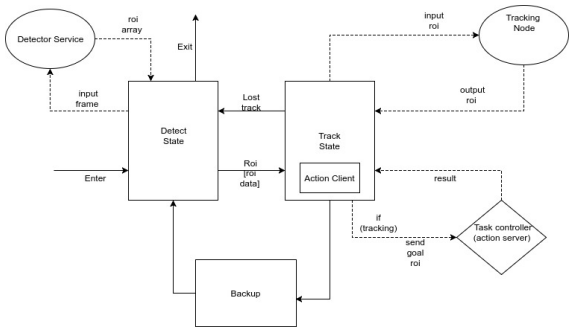

Fig 5. Buoy task state machine

D. Simulator

This year a simulator was built in order to test vision and control algorithms. The insight to build a simulator came from other teams at the competition last year. The software team took advantage of the open source underwater simulator UWsim [13] for marine robotics research and reconfigured it to simulate ARVP's robot. Using the simulator is useful for testing the entire software stack together, makes debugging control logic easier and helps new members learn ROS.

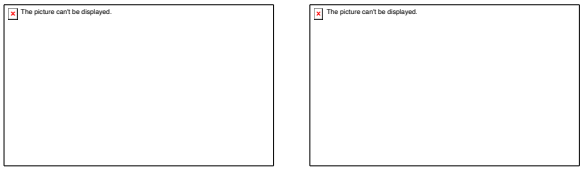

Fig 6. [Left] Simulator overview showing full course [Right] Unity simulator showing three buoys

However, the image quality of the simulator was not sufficient to be used as training data when it comes to deep learning and realistic underwater caustics. Therefore, an additional simulated scene was built using the Unity Game Engine. The high resolution and fast rendering comes in handy and helped generate synthetic images. Fig. 6 [Right] shows an screenshot from the Unity scene.

III. MECHANICAL

ARVP's previous autonomous underwater robot, AquaUrsa, was retired after 4 years and three major rebuilds. Even though AquaUrsa had shown fantastic reliability within the last few years, signs of fatigue and material failure led the mechanical team to the retirement decision in 2016. A subteam was created early that year dedicated to designing a new robot for Robosub 2017. In December the robot's design was finalized, the engineering calculations were completed and the robot was named Auri.

Inspired by the fictional spaceships TIE Fighters from the movie franchise Star Wars, an octagonal outline was given to Auri. In Auri's design process, the team aimed for keeping AquaUrsa's best characteristics and improving the weaknesses. The aluminum frame and the transparent acrylic hull were two of the most important characteristics that were passed on to Auri. Three subassemblies were also successfully integrated into Auri without any changes from when they were used on AquaUrsa (battery enclosures, torpedo assembly and the marker droppers). With 6 degrees of freedom as compared to 5 in AquaUrsa, a 30-pound drop in weight to 60 pounds and a significantly cheaper cost of manufacturing, Auri is without a doubt the most incredible underwater robot that ARVP has ever designed, as shown in Fig. 8.

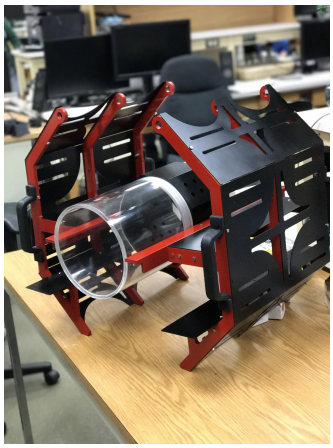

Fig 8. Auri, all mechanical components assembled

A. Hull

The hull for the new robot was completely redesigned. The best parts of the old design were kept in mind, but new innovative ideas were also incorporated to solve issues from previous years. The final design is strong, convenient, practical, and aesthetically pleasing. It is composed of a central aluminum section from which the electronics trays are supported and two acrylic tubes on either side which cover and house the trays as seen in Fig 9. The elegant, clear ¼" acrylic tubes allow for both amazing visibility of the electronics trays and easy access as the tubes can quickly be removed to expose the trays. This means that the trays, although easily

removed themselves, can be worked on without detaching them from the robot. The inner diameter of the tubes is 7.5", which is much smaller than that of the previous hull. This was chosen to reduce the buoyancy of the robot and thus reduce the weight required to sink it. The end caps are also disks of clear acrylic to provide clear visibility for the onboard cameras. The cylindrical shape of the acrylic allows for even pressure distribution to reduce stress and the octagonal shape of the aluminum section provides multiple flat surfaces for easy mounting of components. Aluminum was chosen for the central section because of its non-magnetic property so it would not cause a magnetic interference with any of the electrical components. It is also very easily machined, allowing for this custom octagonal shape to be made. The flat surfaces of the central section allow for subconn connectors and cable penetrators to be mounted for connection between the electrical boards inside the hull and the components outside of it. The cylindrical steps on either side of the aluminium allows for two sets of o-rings to be mounted to provide a watertight seal on the hull. There is also versatility in the orientation of the electrical trays as they can slide into the hull in either the horizontal orientation or the vertical orientation depending on current preference.

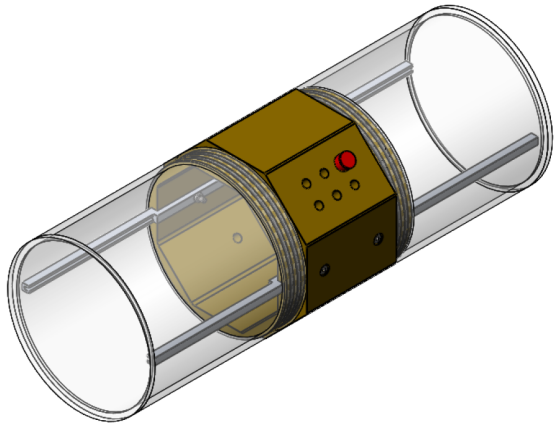

Fig 9. Aluminum hull with acrylic end caps solidworks model

B. Frame

Auri's frame was designed to be more compact, functional, and aesthetically pleasing than ARVP's previous robot. The hull is friction-fit with two complete octagonal rings that are bolted to two L-bars. Attached to these bars are six aluminum ribs, making up the two wings. All components are located inside the wings, providing protection during transportation. Moreover, portability is increased due to four rubber handles attached to the ribs. Bolted to the ribs are multiple trays and side panels. The trays and panels allow for the easy attachment and removal of a variety of components, including torpedoes, thrusters, and marker droppers. The new frame design embodies compactness without sacrificing functional space; this allows for mounting of future mechanisms such as a cooling system or mechanical arm.

C. Battery Enclosures

Auri has two separate battery enclosures, which rest by the hull on aluminum sheets that are mounted to the frame.The battery enclosure is made out of 3.5-inch acrylic cylinders, which is sealed at both ends with aluminum o-ring flanges. The caps of the assembly are designed with 1/2-inch acrylic ends.

D. Marker Release Mechanism

Auri has been equipped with two marker droppers located underneath the pressure hull. The markers themselves are torpedo shaped steel tubes fitted with acrylic fins to ensure stability and optimum accuracy. The marker release mechanism used involves holding the steel markers in place by a magnet. When the target area is identified by the interior cameras, a waterproof servo will move the magnetic field away from the dropper causing it to fall onto the target area. The component housing was 3D printed out of ABS plastic to ensure that the magnetic nature of the system is not compromised by other ferromagnetic metals. This also makes for a simpler machining process.

E. Torpedoes

The torpedo launching module was designed to occupy the least amount of space while delivering the required pressure to propel the torpedoes. This was accomplished using CO2 cartridges that are small as compared to an air tank. The torpedo launching module consists of a CO2 bucket changer that allows for the quick replacement of the cartridges. The bucket changer is directly mounted onto an on/off ASA regulator. This design is rigidly mounted to Auri with the mounting plate from the solenoid valve and eliminates the use of macroline. Mounted on both

solenoid valves is a solenoid-to-tube connector that is press fitted with a 123mm stainless steel pipe.

IV. ELECTRICAL

This year, the electrical team's main focus was to integrate all of the dependable systems from AquaUrsa onto Auri, along with a multitude of upgrades. Since Auri is much smaller, revisions have compensated for this change in size without sacrificing overall performance. Additionally, Auri is now equipped with an array of voltage measuring devices and environment sensors such that Auri's health can always be monitored. Some of the main projects completed this year include: an upgraded power board to supply all of the electronics inside the hull, hydrophone filtering and amplification to be used for sonar, an improved actuator control board, battery and voltage monitoring circuits, internal environment sensors and a simplified motor board, just to name a few. All of these systems fit inside a small hull, shown in Fig 9. Auri was designed with modulation and future advancement in mind, where all of the essential circuit boards come with additional room for expansion. This allows the easy addition and removal of peripheral systems, so that Auri is always prepared for the next big challenge.

Fig 10. Exposed Auri Showing Internal Systems

A. Power Regulation

The new power regulation board was meant to be a near drop-in replacement the board used in AquaUrsa, meaning that it needed to supply power on 12V, 5V, and 3.3V rails and it needed to be controllable using a single pole remote switch. Beyond those specifications, the design of the new board began to deviate from that of the old board to reflect new or upcoming robotic requirements. This included higher power output, especially on the 5V and 3.3V rails. Other requirements included reverse input voltage polarity protection and current sensing. A figure of the power board can be seen in Fig. 10.

i. Switching Voltage Converters

Three switching converters manufactured by Murata Power Solutions are chosen to power the 12V, 5V, and 3.3V rails. The converters can supply 120W, 100W, and 100W respectively which gives the board an overall peak power output rating of 320W [15]. These units accept input voltages ranging from 18V to 75V, provide isolated outputs, and include ON/OFF control topologies and voltage trimming capabilities. Each device uses the standard "eighth-brick" DC-DC converter package.

In the datasheets, it is suggested that excessive input inductance can lead to significant output voltage ripple and can be mitigated with low ESR filtering capacitors. As such, the board is designed to offer the option of adding ceramic capacitors on the input and output nodes of the converters to reduce output ripple. It should be noted that the datasheets cautions against adding excessive output capacitance to the converter output rails since it can lead to instability in the converter's internal control system. Specifically, it states that the total capacitive load for each rail must not exceed 4700µF [15].

ii. Reverse Input Polarity Protection Circuit

Since the voltage converters to not have any built-in reverse polarity protection, an external circuit is added to provide this layer of protection. It is centered around Q1, a p-channel MOSFET, which acts as a switch that turns on when the input polarity is positive and turns off when the polarity is negative. The p-channel style circuit was selected due to its good balance between efficiency and part count [16]. The IPP120P04P4L03AKSA1 p-channel mosfet, manufactured by Infineon Technologies, was chosen in this design primarily for its very low R_{DS} of 3.4mΩ to minimize power losses as much as possible [17]. A 10V Zener diode, represented by D1 in the schematic, is used to hold V_{GS} at -10V during the ON state. This is the optimal gate-source voltage for operating the mosfet [17].

When operating at peak power output, the converters would draw approximately 18A of current from the battery and through Q1 which would dissipate about 1.1W of heat and would have a temperature rise of about 70°C above ambient. A TO-220 compatible heatsink could be used to lower the temperature rise, though it is unlikely that the total power output of the regulation board would reach peak levels continuously.

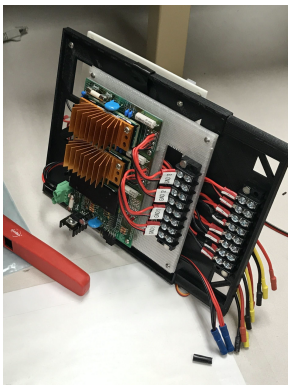

Fig 11. Power Board Mounted on 3D Printed Tray

iii. Current Sensing

Low resistance, precision shunt resistors are used to measure output currents. By measuring the voltage drop across these resistors, the current flowing through them can be calculated. 4±1%mΩ, 4W resistors were selected in this design, which will dissipate up to 1.6W of heat when 20A of current is drawn from a converter. Thanks to the voltage trimming capabilities of the converters, the voltage drop across the shunt resistors will not affect the final output voltage as the converters will automatically correct for it.

iv. Converter ON/OFF Control Circuit

The selected UWE switching converters have a negative logic ON/OFF control scheme, meaning that when the ON/OFF control pin (RC in the schematic) is floating, it will turn off. If this pin is pulled to ground, or in this design to the negative battery terminal, it will turn on. As per the recommendations found in the UWE datasheets, an open-collector control circuit is used in the design to control the converters [15].

v. LED Indication

LEDs are used to indicate if the battery voltage is applied to the inputs of the converters or if the output rails are energized. Series connected resistors to limit current and its values can be determined during production to achieve a desired brightness.

vi. Fuse Selection

The UWE datasheets recommend using 20A fast-blow fuses on the input side of the converters, however no readily available 5x20mm cartridge type fast-blow fuse of that rating could be found. Instead, slow-blow fuses were carefully selected by studying their average time current curves so that at 20A it would blow within 10 seconds [19]. As such, 8A 215 series Littelfuse slow-blow fuses are selected for individual converter protection. A single 10A fuse of the same series is selected for protecting the battery, which blows after 1 second at 30A and 100 seconds at 20A.

vii. Input/Output Connectors

The battery connector is a screw type 2 position, 32A rated terminal block by Phoenix Contact [20]. Due to PCB layout constraints, polarity markings are on the bottom of the board. The battery voltage can be measured by reading the voltage across the two pins in JP7.

Wire pads are used as output rail connectors as is used in the currently used board. The holes are approximately 1.3mm in diameter and can have wires up to 17AWG soldered into it. A 2.54mm pitch male pin header can supply 12V, 5V, and 3.3V to an expansion board if desired.

B. Voltage Monitoring

The battery monitoring system is designed to monitor the voltages of the four batteries powering the robot and display them on an LCD in real time. The main system is incorporated into the power board; however, the LCD and a hall sensor are separate. The system uses two INA3221s to monitor the voltages of the batteries and the current from the motors. Each of the INA3221s can monitor up to three channels and detect load voltage, bus voltage, and current from each channel using small current sensing resistors. The INA3221s have several warning features such as power-valid, warning, and critical that are active based on the voltages measured. These features have not yet been coded or tested, but the wiring is there for future use. The system uses a teensy 3.2 to run the INA3221s, a standard 16x2 LCD, a shift register, and a hall sensor. The teensy was chosen due to its small size, low cost, and compatibility with Arduino software. To reduce the number of LCD pins required on the teensy from six to three, a 74HC595N shift register was added to the board. To conserve power, the backlight of the LCD can be switched on and off using a DRV5033 digital omnipolar hall switch which will be mounted near the outside of the hull. In summary, the INA3221s measure the voltage and current values which are collected by the teensy. This data can be used by the software team to determine exactly when voltage or current drops occur. The teensy also sends the voltage data to the LCD mounted next to the hull which displays the values when a magnet is present near the hall sensor.

C. Internal Environment Sensing

i. Humidity and Temperature Sensor

HoneyWell's HIH7120 is a dual humidity and temperature sensor the purpose of which is to monitor humidity of the air inside the hull to possibly detect leaks and prevent equipment failures. The temperature sensor will be used to detect the internal temperature of the submarine so that equipment failure due to overheating may be avoided. This sensor was the best choice for several reasons including its digital output. The sensor outputs the data over I2C after the master device sends a measurement request otherwise the sensor is in a low power mode which conserves energy. The sensor also has an unlimited moisture sensitivity level meaning that the sensor won't have to be replaced very often. This sensor also boasts a fast response time which will allow the submarine's computer to dynamically monitor the humidity levels and be able respond quickly given a rapid change in the internal environment. While the sensor isn't the most accurate, for the purposes of detecting a change in humidity it will work fine. Furthermore, the sensor's small size will allow for it to be integrated into a smaller pcb conserving valuable space in the inside of the submarine. Finally, the sensor's relatively low cost will be a benefit if the circuitry is damaged or more than one sensor is needed, inside the quad or for going through prototypes of the board as soldering the sensor to the board is tricky due to its small size.

ii. Pressure and Temperature Sensor

NXP MPL3115A2 is a dual pressure and temperature sensor. The pressure sensor is an absolute piezoresistive sensor, the purpose of which is to monitor the pressure inside the hull for any sudden changes which would indicate a hull breach or failure. This sensor was chosen also because if it's digital I2C interface. This allows it to be directly interfaced with a microcontroller making the pcb design smaller and more compact. Next the sensor is quite accurate and has a quick response time allowing for the internal pressure to be dynamically monitored at a high degree of accuracy. This will allow the detection of minor changes in the pressure very quickly and allow the submarine to detect possible hull failures. This sensor is also quite small and low powering which offers the same advantages as described for the humidity sensor. Finally, the sensor is even lower cost than the humidity sensor allowing for multiple sensor to be purchase for multiple measurements prototypes and replacements.

D. Actuator Board

The actuator board of Auri was designed to control all output devices on the robot other than the thrusters and motors. It features a Teensy 3.2 microcontroller that receives instructions from the ODROID via the microUSB port, and its GPIO pins control different components in the board. The board takes power inputs of 5V and 12V from the power board. This board is designed to control the marker dropper actuators, torpedo solenoids as well as the LED indication strip mounted internally inside the hull.

V. BUSINESS

The Business Team was created this year with the goal of transforming ARVP into a club that can compete toe-to-toe against its international competitors. This started by creating a strong financial foundation, driven by a campaign to create value for its sponsors. The team would complete this objective on two fronts, one through community involvement, and two through direct benefits provided through our sponsorship package. Community outreach included high school demonstrations, organizing a monthly robotics conference, ROS Edmonton, at the municipal startup accelerator, and community volunteerism. The team put on a crowdfunding campaign through USEED that raised over $18,000. A business plan, budget, and monthly accounting balance sheets, gave ARVP a new level of accountability too.

Fig 12. Advertisement for monthly ROS Edmonton event, giving tutorials on ROS and topics related to robotics and autonomy.

VI. Experimental Results

ARVP began work on vision, and simulation in September 2016. By the beginning of this year, we started testing on the simulator. The simulator has allowed for testing the entire software system out of the pool. Auri was finished in the middle of June. Before that, testing was done on the last generation AquaUrsa starting in April.

APPENDIX A - REFERENCES

References

[1] K. Iqbal, M.Odetayo, A. James, R. Salam and A. Talib. *Enhancing The Low Quality Images Using Unsupervised Colour Correction Method.* International Conference of Systems, Man and Cybernetics, Istanbul, Turkey, 2010, pp. 1704-1709.

[2] R. Buchner and D. Misra. A Synthesizable VHDL Model of the Exact Solution for Three-dimensional Hyperbolic Positioning System. VLSI Design, 2002, Vol. 15 (2), pp. 507-520.

[3] OpenCV. [Online.] Available: http://opencv.willowgarage.com/.

[4] OpenCV4Tegra. [Online.] Available: http://tinyurl.com/gv3fop3.

[5] Robot Operating System. [Online.] Available: http://www.ros.org/.

[6] ROS actionlib. [Online.] Available: http://wiki.ros.org/actionlib.

[7] ROS rqt. [Online.] Available: http://wiki.ros.org/rqt.

[8] ROS dynamic reconfigure. [Online.] Available: http://wiki.ros.org/dynamic reconfigure.

[9] ROS Smach. [Online.] Available: http://wiki.ros.org/smach.

[10] V. Pătrăucean *et al.*, "A parameterless line segment and elliptical arc detector with enhanced ellipse fitting." in *European Conference on Computer Vision*, Amsterdam, NL, 2012, pp. 572-585.

[11] J. Redmon, A. Farhadi. *YOLO9000: Better, Faster, Stronger.* arXiv preprint arXiv:1612.08242, 2016.

[12] A. Tao, J. Barker, S. Sarathy. *DetectNet: Deep Neural Network for Object Detection in DIGITS.* [Online.] Available: https://devblogs.nvidia.com/parallelforall/detectnet-deep-neural-network-object-detection-digits/

[13] ROS UWSim [Online.] Available: http://wiki.ros.org/uwsim

[14] A. Shafaei, J. Little, M. Schmidt. *Play and Learn: Using Video Games to Train Computer Vision Models.* arXiv:1608.01745v2 [cs.CV] 15 Aug 2016

[15] Murata Power Solutions, "UWE-100-120W Series Wide Input, Isolated Eighth-Brick DC-DC Converters," UWE-12/10-Q48PB-C datasheet. 2017.

[16] Infineon Technologies AG, "Automotive MOSFETs Reverse Battery Protection," Application Note.

[17] Infineon Technologies AG, "OptiMOS® -P2 Power-Transistor," IPP120P04P4L03AKSA1 datasheet. May 2015.

[18] Texas Instruments, "INA3221 Triple-Channel, High-Side Measurement, Shunt and Bus Voltage Monitor with I2C- and SMBUS-Compatible Interface," INA3221 datasheet. March 2016.

[19] Littelfuse, "Axial Lead & Cartridge Fuses," 215 series slow blow fuse datasheet. January 2017.

[20] Phoenix Contact, "MKDS 5/ 2-7,62 PC Terminal Block" MKDS 5/ 2-7,62 datasheet. January 2011.

APPENDIX B- ENLARGED MATERIALS

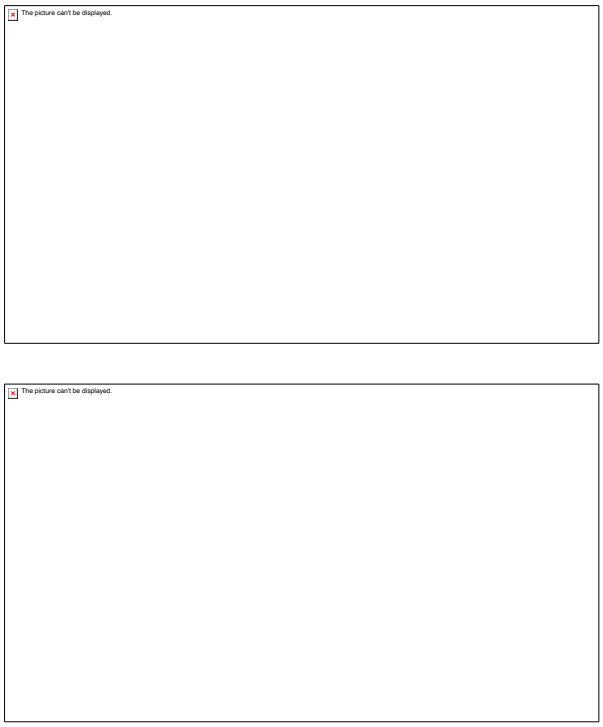

Fig A1. [Top] - Detection with caustics
[Bottom] - Detection from far away

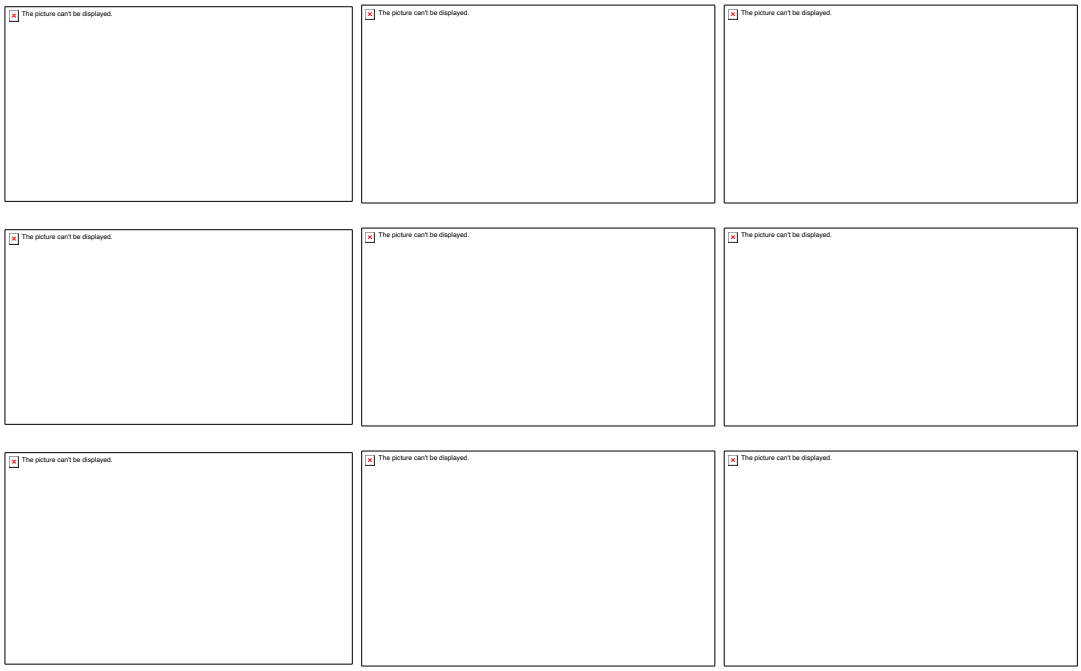

Fig. A2. [Top row] -Deep learning Object Detection with caustics on the buoy, [Middle row] - Detection in darker condition, [Bottom row] - Detection from far away and with poor visibility